

# Chorus: Harmonizing Context and Sensing Signals for Data-Free Model Customization in IoT

Liyu Zhang

The Hong Kong University of  
Science and Technology  
Hong Kong, China  
lzhangcx@connect.ust.hk

Yejiu Liu

The Hong Kong University of  
Science and Technology  
Hong Kong, China  
yliutb@connect.ust.hk

Kwun Ho Liu

The Hong Kong University of  
Science and Technology  
Hong Kong, China  
khliuae@connect.ust.hk

Runxi Huang

The Hong Kong University of  
Science and Technology  
Hong Kong, China  
rhuangbj@connect.ust.hk

Xiaomin Ouyang

The Hong Kong University of  
Science and Technology  
Hong Kong, China  
xmouyang@cse.ust.hk

## ABSTRACT

A key bottleneck toward scalable IoT sensing is how to efficiently adapt trained AI models to new deployment conditions. In real-world IoT systems, sensor data is collected under diverse and changing contexts, such as varying sensor placements or ambient environments, which can significantly alter signal patterns and degrade downstream performance. Traditional domain adaptation and generalization methods often ignore such contextual information or incorporate it in overly simplistic ways, making them ineffective under unseen context shifts after deployment.

In this paper, we propose Chorus, a *context-aware, data-free model customization* approach that adapts models to unseen deployment conditions without requiring target-domain data. The key idea is to learn effective context representations that capture how contextual factors influence sensor data, and then use these representations as structured priors for context-aware customization under unseen shifts. Specifically, Chorus learns a shared sensor–context latent space through bidirectional cross-modal reconstruction on unlabeled sensor–context pairs, and regularizes the context embedding space to obtain compact and generalizable context representations. Building on the aligned representations, Chorus trains a lightweight gated head with limited labeled data to exploit context priors during inference, and introduces a context-caching mechanism that reuses cached context representations when no context shift is detected, thereby reducing inference overhead on smartphones.

Experiments on IMU, speech enhancement, and WiFi sensing tasks under diverse context shifts show that Chorus outperforms state-of-the-art baselines by up to 20.2% in unseen contexts, with cached inference latency close to

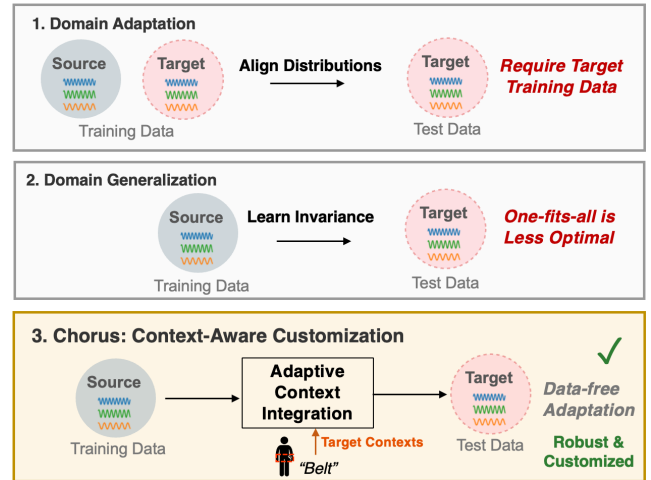


**Figure 1: Chorus aligns sensor signals and lightweight deployment context descriptions in a shared latent space for data-free model customization under unseen context shifts.**

sensor-only deployment on smartphones, while maintaining stable performance under continuous real-world context transitions<sup>1</sup>. A video demonstration of Chorus’s performance in real-world deployment is available at <https://youtu.be/ZBdro0jPNkE>.

## 1 INTRODUCTION

Many Internet of Things (IoT) and mobile sensing applications rely on heterogeneous sensors such as IMUs, microphones, and wireless radios to perceive the physical world for downstream analysis or control tasks [11, 21, 25, 32].

<sup>1</sup>The source code for Chorus will be released once the paper is accepted.

However, these sensors often operate under rapidly changing *contexts*, where operational and environmental conditions induce substantial distribution shifts [13, 15, 32]. In wearable sensing, for instance, sensor placement encodes critical contextual information: an accelerometer trace differs markedly when a smartwatch is worn on the wrist versus clipped to the arm [30]. Similarly, in wireless sensing, Wi-Fi Channel State Information (CSI) signals vary significantly across physical environments, such as line-of-sight versus through-wall settings [14, 18]. In machine learning, such physical *context shifts* induce statistical *domain gaps*, where data distributions differ substantially across contexts [44]. As summarized in Figure 1, domain adaptation aligns source and target distributions but assumes access to target data, whereas domain generalization learns a single invariant model from source data alone and often suppresses domain-specific structure that remains important for target performance. By contrast, Chorus leverages only deployment-time context descriptions—readily obtained from system metadata, lightweight user setup, or mobile context detectors and sensing front-ends [16, 36]—to customize prediction models for the target context without requiring target-domain samples.

However, existing approaches for handling such context-induced domain gaps have their own limitations. Domain generalization aims to learn domain-invariant features from multiple source domains, but this often suppresses context-sensitive information that remains crucial for challenging target conditions [9, 40]. Conversely, domain adaptation, few-shot fine-tuning, and test-time adaptation (TTA) require access to target-domain data after deployment and introduce non-trivial on-device model update overheads [4, 7, 10, 17, 31, 35]. This assumption is particularly problematic in mobile and IoT sensing, where computing resources are limited and contexts may shift significantly even within seconds. In such scenarios, collecting target data and retraining models is often impractical—especially for real-time applications. These constraints motivate the setting we target: *no access to target-domain data during training and no model retraining after deployment*. Although recent works have begun incorporating context into sensing pipelines, they typically treat context as static side information, rule-based conditions, or selectors for expert subnetworks—rather than explicitly aligning semantic context with physical sensor signals in a unified representation space [20, 46]. As shown in our motivation study (Section 3), the lack of such alignment is a key reason why naive context injection fails to remain reliable under unseen context shifts.

To address these challenges, we propose Chorus, a context-aware framework for data-free model customization in IoT sensing applications. The key idea, illustrated in the bottom

panel of Figure 1, is to transform easily available deployment-time context descriptions into effective representations that capture context-dependent variation in sensor data patterns, and then use these representations as structured priors for context-aware customization under unseen shifts.

Specifically, Chorus uses a two-stage training scheme to achieve this goal using abundant unlabeled data and a small amount of labeled data. In the first stage, Chorus trains sensor and context encoders via bidirectional cross-modal reconstruction, where the model reconstructs sensor and context features from the paired modality. This process aligns sensor and context representations in a shared latent space, allowing the encoder to capture how sensor patterns vary across physical contexts. We further introduce a regularization term that compacts and separates context embeddings in the latent space, improving generalization to unseen contexts. In the second stage, Chorus freezes the encoders and trains a lightweight gated head with limited labeled data, which adaptively modulates the influence of sensor and context embeddings for each instance. To further reduce inference latency, we introduce a context-caching mechanism that reuses cached context representations across consecutive samples and refreshes the cache when a context shift is detected.

Our experimental evaluation on three public datasets under 15 diverse context conditions, including 5 IMU placements, 5 acoustic environments, and 5 WiFi deployments, shows that Chorus outperforms the strongest baseline across all IMU and WiFi shift tiers, with the largest gain of 20.2 percentage points over CACTUS on IMU Low shift, while remaining competitive on speech and achieving the best result under High shift. Evaluations on mobile phones further show that cached inference latency remains close to sensor-only deployment, while context caching reduces latency by 23.6× on iPhone 16 Pro and 29.7× on Xiaomi 14 over the uncached design, making Chorus practical for edge deployment.

In summary, we make the following key contributions:

- We conduct an in-depth motivation study on context shifts in sensing applications, showing that model performance degrades sharply as context shift increases and that naive context integration strategies are not reliable across unseen deployment conditions.
- We propose Chorus, a context-aware framework for data-free model customization under unseen deployment conditions. Chorus learns effective and generalizable context representations through regularized cross-modal reconstruction, and performs efficient inference-time customization with a lightweight gated head and context caching.
- Extensive evaluations across three sensing modalities and 15 context conditions show that Chorus consistently outperforms strong baselines, especially under larger unseen context shifts, while maintaining low cached inference

overhead and stable performance under continuous real-world context transitions.

## 2 RELATED WORK

**Domain Adaptation.** Recent mobile sensing work explores unsupervised DA (e.g., M3BAT [19]), few-shot adaptation (e.g., TS2ACT [39]), test-time adaptation (e.g., OFTTA [37]), and related source-only pre-train/fine-tune pipelines such as TS-TST [43]. Despite improving robustness, these methods each face critical bottlenecks in edge deployments. Few-shot methods implicitly assume a relatively stable target domain, whereas mobile contexts often shift within seconds. Test-time adaptation faces a latency–energy trap: it must buffer deployment streams and perform on-device backpropagation, introducing unacceptable cold-start delays precisely when physical shifts occur. Ultimately, these target-dependent update assumptions are poorly matched to highly dynamic mobile sensing. By contrast, Chorus targets strictly data-free customization for unseen deployment contexts.

**Domain Generalization.** Domain generalization removes the need for target data by learning representations that transfer across unseen domains [45]. Representative approaches include adversarial schemes such as DANN [5] and ContrasGAN [24], as well as recent sensing systems such as DGSense [46]. However, these methods primarily pursue domain-invariant representations, which can inadvertently suppress context-specific cues that remain useful under strong shifts. By contrast, Chorus does not discard context information; instead, it treats deployment-time context as a structured prior, aligns it with sensor signals in a shared latent space, and exploits it adaptively at inference time.

**Context-aware Learning.** Context-aware sensing has shown that side information can improve robustness [6, 32], and CACTUS is a representative recent system in this direction [23]. However, CACTUS follows a specialist architecture in which model structure grows with the number of context-specific experts, and context is integrated through expert routing or fixed fusion rather than being fundamentally aligned with physical signals. As the number of contexts increases, this expert-specialization design incurs parameter growth and increasing edge cost. By contrast, Chorus performs generative sensor–context alignment in a regularized shared latent space and then uses a lightweight inference-time head to exploit these aligned priors, yielding a unified  $O(1)$  generalist architecture for context-aware customization even when the target context is unseen during training.

## 3 A MOTIVATION STUDY

### 3.1 Performance under Context Shifts

A key challenge for deep learning-based sensing applications is the performance degradation caused by shifts between

training and testing contexts. To systematically analyze this, we evaluate model performance using IMU data from 10 subjects in the public Shoaib dataset [28] for human activity recognition (HAR). The task is to classify six human activities across different on-body sensor placements (e.g., *Wrist*, *Left pocket*, *Right pocket*, *Upper Arm*, and *Belt*).

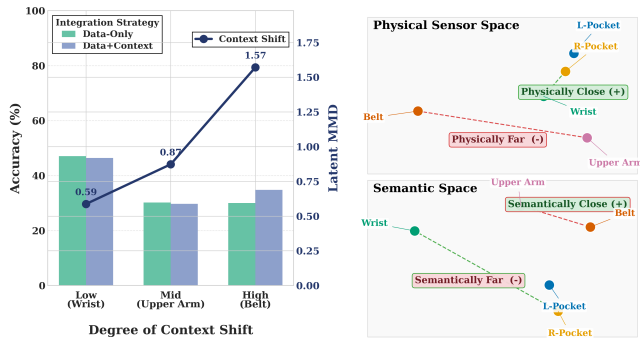
We quantify the degree of context shift between training and testing data using a latent MMD metric [8], computed on sensor representations extracted by a source-only vanilla autoencoder trained only with reconstruction loss. A higher latent MMD score indicates a larger distributional gap and thus a greater context shift. Using “Left pocket” and “Right pocket” as the source training contexts, we categorize three levels of shift for the remaining placements: *low* (“Wrist”, latent MMD = 0.587), *mid* (“Upper Arm”, latent MMD = 0.873), and *high* (“Belt”, latent MMD = 1.571).

As a reference, we first consider a *Data-Only* approach that predicts activities solely from sensor inputs without using any explicit context information. As shown by the Data-Only bars and the latent MMD curve in Figure 2(a), the Data-Only model drops sharply as the latent context shift grows from Wrist to Upper Arm and remains low under the high-shift Belt setting. To address this degradation, a straightforward idea is to integrate sensing context into the model. We compare the *Data-Only* approach against a *Data+Context* strategy, which integrates pre-trained language embeddings of the placement descriptions (via MiniLM-v2 [38]) using simple addition.

However, naively injecting context does not uniformly improve accuracy. In the low-shift *Wrist* scenario, adding context slightly reduces accuracy from 47.1% to 46.4%. A similar pattern appears in the mid-shift *Upper Arm* scenario, where accuracy drops from 30.2% to 29.7%. Only in the high-shift *Belt* context does naive context fusion become beneficial, improving accuracy from 30.0% to 34.8%. This pattern shows that simple context fusion is unstable under light-to-moderate shift and becomes useful only when the deployment shift is severe enough that sensor evidence alone is no longer reliable.

### 3.2 Understanding Context Injection

To understand why naive context injection behaves so inconsistently, we compare the pairwise relationships among the five placement contexts in two independent spaces. In the latent sensor space, we measure pairwise distances using latent MMD between context-specific IMU representations extracted by a source-only vanilla autoencoder. In the semantic context space, we encode the same placement labels using MiniLM-v2 [38], compute pairwise cosine distances, and project both distance matrices with multidimensional scaling (MDS) [2].



**(a) Performance across context shifts.** **(b) Topological mismatch between sensor and context spaces.**

**Figure 2: Motivation study on context shifts and naive context integration.**

Figure 2(b) reveals a clear topological mismatch between these two spaces. Contexts that are physically similar can be pushed far apart in the semantic space, while physically distinct contexts can be grouped together by linguistic similarity. For example, *Wrist* remains relatively close to the pocket placements in the latent sensor space, consistent with their shared limb-motion dynamics, yet it is placed much farther away in the semantic space. In contrast, *Upper Arm* is noticeably farther from the pocket placements and *Belt* is the most distant in the latent sensor space, while the semantic embedding still tends to group these coarse-grained body-worn locations together. As a result, the semantic prior distorts the physically meaningful neighborhood structure that the sensing model should rely on. When context is injected through naive addition, the model must fuse misaligned representations, which leads directly to the unstable behavior observed in Figure 2(a).

### 3.3 Summary

Our motivation study highlights two key insights that drive the design of Chorus:

- The performance of sensing models degrades significantly as the degree of context shift increases. Although incorporating context can be beneficial, naive integration strategies such as simple additive fusion remain unreliable under unseen contexts.
- Raw text embeddings of context descriptions exhibit a severe topological mismatch with sensor embeddings: physically similar contexts may appear far apart in semantic space, while physically distinct contexts may be spuriously clustered together.

Therefore, robust model customization requires effective sensor-context alignment as the foundation. Context descriptions and sensor signals must first be mapped into a unified and compact representation space that preserves physically

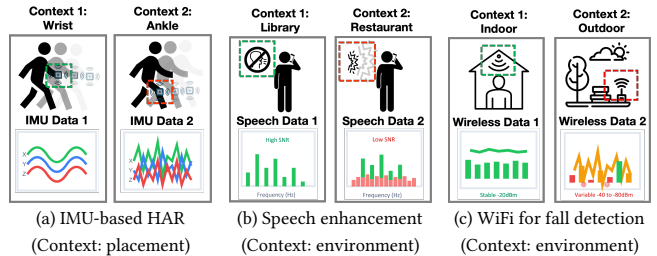


**Figure 3: Context shifts in different sensing applications.**

meaningful neighborhood structures. Once this aligned latent space is established, we can develop adaptive context integration approaches that leverage the appropriate context prior more reliably at inference time.

## 4 SYSTEM OVERVIEW

### 4.1 Applications and Challenges

Chorus targets IoT sensing applications where sensor data is collected under diverse and dynamic contextual conditions. Here, *context* [3] refers to environmental and operational factors, such as device placement, ambient noise, or user mobility, that systematically affect sensor patterns. As illustrated in Figure 3, such context shifts arise in wearable HAR, speech enhancement, and WiFi sensing.

In human activity recognition with wearables, on-body sensor placement (e.g., wrist vs. ankle) is a critical context that substantially changes IMU signal patterns. Even for the same activity such as “walking,” accelerometer and gyroscope readings exhibit different statistics across placements. In speech enhancement, environmental context, such as a quiet office versus a busy street, introduces different ambient noise patterns in raw audio. In wireless sensing, user mobility and physical environment significantly affect Wi-Fi Channel State Information (CSI), leading to context-dependent multipath fading and Doppler effects.

Across these applications, contextual variation raises three challenges. First, the model should generalize to unseen contexts, since collecting sufficient labeled data for every deployment condition is impractical. Second, the relationship between context and sensor shifts is complex and task-dependent, which requires effective context representations rather than naive context injection. Third, many IoT sensing tasks are latency-sensitive, calling for lightweight customization at inference time.

### 4.2 Problem Formulation

The goal of Chorus is to enable data-free context-aware model customization for unseen deployment contexts. The model is trained solely on source-context data and deployed directly to unseen target contexts without any target-domain

samples. During inference, it incorporates lightweight context information from the target environment, such as placement, room type, or device configuration, which can typically be logged automatically or provided through simple user input. Since collecting labeled data for every possible context is impractical in many IoT applications, Chorus instead leverages abundant unlabeled sensor–context pairs and a small amount of labeled source data to learn effective context representations and their influence on sensor patterns.

### 4.3 System Architecture

The design of Chorus is motivated by the key insight from Section 3 that naive context integration is unreliable under unseen context shifts. The key idea is to transform lightweight deployment-time context descriptions into effective representations that capture how sensor patterns vary across physical conditions, and then use these representations as structured priors for context-aware customization. Figure 4 shows the overall system architecture.

Chorus first learns effective and generalizable context representations from unlabeled *source* sensor–context pairs collected under diverse conditions. The context descriptors, such as environmental metadata, placement tags, or device-state annotations, are lightweight side information obtained from system metadata, lightweight user setup, or context-sensing front-ends, and are expressed as short language descriptions before being encoded into compact context embeddings. Chorus then trains sensor and context encoders via *bidirectional cross-modal reconstruction*, which reconstructs sensor signals from context descriptions and context from sensor signals. This process aligns sensor and context representations in a shared latent space, allowing the model to capture how sensor patterns vary across physical contexts. In addition, Chorus applies a regularization term that compacts and separates context embeddings to improve generalization to unseen contexts.

In the second stage, Chorus performs lightweight supervised customization without using target-domain data. It freezes the pre-trained encoders as feature extractors and trains only a small gated head on limited labeled source data, allowing the model to exploit the aligned sensor and context embeddings at inference time. To further reduce runtime latency, Chorus employs a dynamic context cache that reuses cached context embeddings across consecutive samples and refreshes them only when a context shift is detected. In this way, Chorus thus enables data-free customization under unseen deployment conditions without retraining after deployment.

## 5 DESIGN OF CHORUS

Chorus first learns context representations through regularized cross-modal reconstruction, forming a shared latent space between sensor signals and deployment context. Building on this aligned space, Chorus then employs a lightweight gating module to adaptively integrate context information under different context shifts. Chorus also features a dynamic context caching mechanism to further reduce inference overhead.

### 5.1 Bidirectional and Regularized Context Representation Learning

In the first stage of Chorus, we train a context-aware sensor encoder  $f_{sensor}$  and a context encoder  $f_{context}$  on unlabeled sensor–context pairs, with the goal of learning a feature space grounded in the underlying physical context. Suppose  $(x_s, c_s)$  denotes an unlabeled sensor–context pair from the source domains, where  $x_s$  is a sensor segment and  $c_s$  is its associated pre-computed context embedding derived from a short language description. For example, in HAR, this context may be an on-body placement such as “Left pocket”, “Wrist”, or “Belt”, while in speech enhancement it may be an acoustic environment such as “Kitchen”, “Bus”, or “Office”. We map these two inputs into a latent space as

$$z_x = f_{sensor}(x_s), \quad z_c = f_{context}(c_s).$$

Here  $f_{sensor}$  is a modality-specific encoder, such as a 1D CNN for IMU signals or a Transformer/CNN encoder for speech and WiFi features, while  $f_{context}$  is a lightweight context adapter built on top of pre-computed MiniLM-L12-v2 sentence embeddings [38].

*5.1.1 Bidirectional cross-modal reconstruction.* We first map sensor and context embeddings into a shared latent space to capture the relationship between context shifts and sensor pattern variation. In implementation, we combine bidirectional cross-modal reconstruction with within-modal self-reconstruction, so that the latent variables preserve modality fidelity while still enforcing cross-modal alignment. Let  $\hat{x}_{x \rightarrow x}$  and  $\hat{c}_{c \rightarrow c}$  denote self-reconstructed sensor and context features, and let  $\hat{x}_{c \rightarrow x}$  and  $\hat{c}_{x \rightarrow c}$  denote cross-reconstructed features predicted from the opposite modality. We optimize:

$$\begin{aligned} \mathcal{L}_{recon} = & \alpha_{x \rightarrow x} d(\hat{x}_{x \rightarrow x}, x_s) + \alpha_{c \rightarrow c} d(\hat{c}_{c \rightarrow c}, c_s) \\ & + \alpha_{c \rightarrow x} d(\hat{x}_{c \rightarrow x}, x_s) + \alpha_{x \rightarrow c} d(\hat{c}_{x \rightarrow c}, c_s). \end{aligned} \quad (1)$$

Here  $d(\cdot, \cdot)$  denotes a standard reconstruction distance between continuous targets. We use this generic form because both the sensor targets and the context targets are continuous tensors rather than discrete labels; in practice, it is instantiated with standard element-wise regression losses. Such

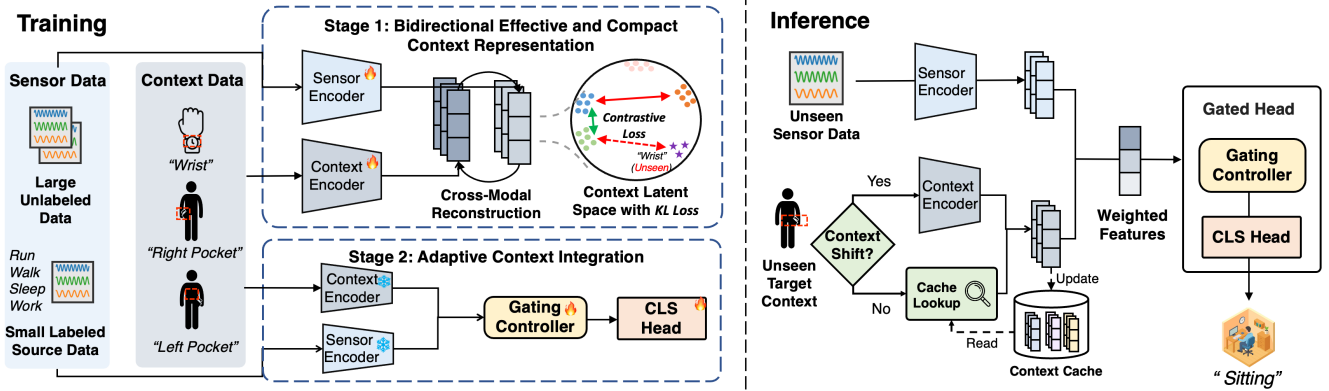


Figure 4: System Overview. Chorus performs regularized cross-modal reconstruction on unlabeled sensor–context pairs to *semantically harmonize* context and sensor embeddings in a shared latent space. It then uses a lightweight gating head to efficiently exploit the context priors for model customization, and a context-caching mechanism for reducing inference overhead.

reconstruction objectives are widely used in multimodal generative models to align heterogeneous modalities in a shared latent space [22, 27, 29, 42]. In our setting, this encourages the latent space to capture both task-relevant structure, such as the movement pattern of a walking activity, and systematic pattern distortions induced by context, such as how the same activity is expressed on the ‘wrist’ versus the ‘belt’. As a result, the sensor embeddings  $z_x$  become informative about context, allowing the downstream gated head to modulate the influence of sensor and context information, while the context embeddings  $z_c$  form compact and reusable representations for each placement or environment.

5.1.2 *Latent regularization for context embeddings.* As shown in Figure 2(b), raw semantic context embeddings do not necessarily preserve physically meaningful neighborhood structure across sensing conditions. Directly reusing these pre-trained language embeddings therefore limits generalization to unseen contexts. To address this issue, we further regularize the latent space to encourage both compactness and inter-context separation. Specifically, the first-stage objective combines reconstruction, latent regularization, and contrastive context separation:

$$\mathcal{L}_{\text{pre}} = \mathcal{L}_{\text{recon}} + \beta \mathcal{L}_{\text{KL}} + \lambda_{\text{sep}} \mathcal{L}_{\text{sep}}.$$

Here  $\mathcal{L}_{\text{KL}}$  is a latent KL regularization term that stabilizes the learned latent distributions during pre-training. It prevents the learned embeddings from drifting toward broad language directions inherited from the pre-trained embedding space, and instead keeps them in a physically grounded region shaped by sensor–context co-occurrence. The separation term  $\mathcal{L}_{\text{sep}}$  is implemented as an InfoNCE-style contrastive loss over context identities: it treats samples with identical

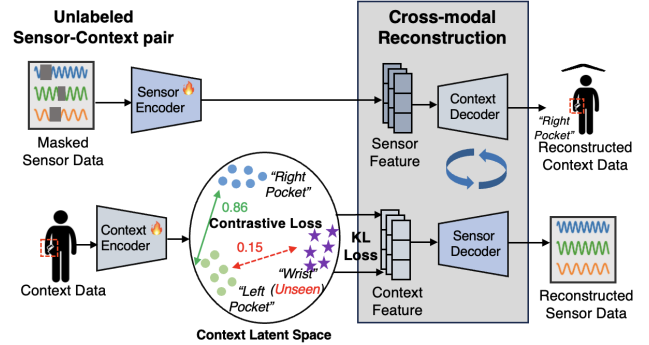


Figure 5: Learning effective context representations through cross-modal reconstruction and latent regularization with context separation.

context IDs as positives and all other context IDs in the mini-batch as negatives. Its role is to explicitly separate different physical contexts and prevent trivial collapse, where multiple contexts are mapped into an overly similar region.

Together, these terms produce well-separated context embeddings that are later used by the gating controller. Combined with the reconstruction objective, they make the context branch more task-specific and more sensitive to physical context variation. In implementation, we may include a small number of auxiliary stabilization terms for specific modalities, but the core pre-training objective is governed by reconstruction, latent regularization, and context separation.

As a result, the pre-trained  $f_{\text{sensor}}$  serves as a context-aware feature extractor whose embeddings encode both task structure and context-induced distortions, while the pre-trained  $f_{\text{context}}$  produces compact, well-separated context representations that can be directly consumed and cached by the adaptive gating head in the second stage.

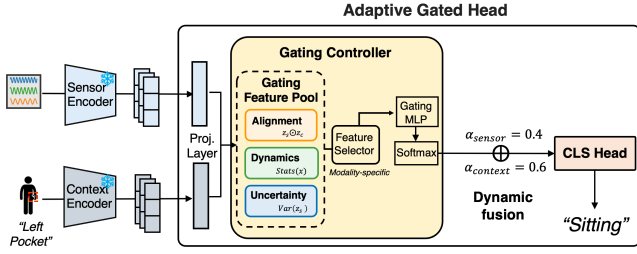


Figure 6: Adaptive context integration with a light-weight gating controller.

## 5.2 Adaptive Gating for Context Integration

In the second stage, Chorus performs lightweight supervised customization on top of the aligned latent space. The gated head does not learn context representations from scratch; instead, it exploits the pre-aligned sensor–context embeddings to activate the appropriate context prior for each input under different sensing conditions. Given a small labeled source dataset  $\mathcal{D}_{s,l}$ , this head learns to balance the contributions of sensor and context information for each input.

**5.2.1 Adaptive Gating Controller.** To effectively capture different aspects of sensor data and context information, the head employs sensor and context projection layers, as shown in Figure 6. To dynamically blend the outputs of the two branches, we introduce a lightweight *Gating Controller* ( $g_c$ ), which maps a compact set of gating features to routing weights over the sensor and context branches [12, 26].

The controller operates on a shared gating feature pool with three types of instantaneous signals: (i) *alignment* features derived from interactions between sensor and context embeddings, (ii) *dynamics* features derived from simple statistics of the current input segment, and (iii) *uncertainty* features derived from the sensor representation [41]. In Figure 6, these cues are illustrated as  $z_s \odot z_c$ ,  $\text{Stats}(x)$ , and  $\text{Var}(z_s)$ , respectively. Because context shifts manifest differently across sensing modalities, Chorus does not enforce the same gating cues across all modalities. Instead, it uses a configurable feature subset selector to activate a modality-appropriate subset of the shared feature pool before gating. In the current implementation, this selector is realized as a simple mask over feature groups, enabling a unified controller architecture while allowing modality-dependent gating inputs.

Given a gating feature vector  $r(x)$  extracted from the current input, the controller applies a small MLP and produces logits over the two branches, which are converted via a softmax into weights

$$\alpha(x) = [\alpha_{\text{sensor}}(x), \alpha_{\text{context}}(x)] = \text{softmax}(g_c(r(x))) \in \mathbb{R}^2.$$

In this way, the gating controller implements instance-wise adaptation to changing contexts instead of using a naive fusion mechanism.

The final representation  $h_{\text{final}}$  is obtained via a weighted sum of the two branch outputs:

$$h_{\text{final}} = \alpha_{\text{sensor}} h_{\text{sensor}} + \alpha_{\text{context}} h_{\text{context}}.$$

This allows the model to increase  $\alpha_{\text{context}}$  when sensor evidence is ambiguous and to rely more on  $\alpha_{\text{sensor}}$  when the patterns are stable. A final task head operates on  $h_{\text{final}}$  to produce the prediction  $\hat{y}$ .

**5.2.2 Training objective for the gated head.** To encourage the gated head to use both branches instead of collapsing to a single one, we add a regularization loss that promotes balanced branch utilization across each mini-batch, on top of the main task loss. We optimize

$$\mathcal{L}_{\text{custom}} = \mathcal{L}_{\text{task}}(y, \hat{y}) + \lambda_{\text{balance}} \mathcal{L}_{\text{balance}},$$

where  $\mathcal{L}_{\text{task}}$  denotes the task-specific supervision loss, and  $\mathcal{L}_{\text{balance}}$  is a regularization term that discourages the gating controller from collapsing to a single branch across the batch. In our implementation,  $\mathcal{L}_{\text{task}}$  is instantiated as cross-entropy for IMU and WiFi classification, and as a signal-level enhancement loss for speech.

This regularization avoids a trivial solution in which the model always relies on the same branch. To prevent this, we first compute the average gate usage of each branch over a mini-batch of size  $B$ :

$$\bar{\alpha}_k = \frac{1}{B} \sum_{b=1}^B \alpha_k(x_b), \quad k \in \{\text{sensor}, \text{context}\}.$$

We then penalize the deviation of this average usage from a uniform target:

$$\mathcal{L}_{\text{balance}} = \frac{1}{K} \sum_{k=1}^K \left( \bar{\alpha}_k - \frac{1}{K} \right)^2,$$

where  $K$  is the number of branches, and in our setting  $K = 2$ . This loss encourages the average branch usage within a batch to remain balanced, so that the controller learns to exploit both sensor-intrinsic patterns and contextual cues instead of always routing to the same path. The scalar  $\lambda_{\text{balance}}$  controls the strength of this regularization.

## 5.3 Dynamic Context Caching for Inference Optimization

To mitigate the computational overhead of repeatedly encoding context features during inference, we exploit the high temporal locality of context information in real-world streaming scenarios. In typical IoT deployments, contextual descriptors and their resulting embeddings often remain stable across extended sequences of input samples. For example, device placement usually does not change within a session, acoustic environments often persist for minutes, and wireless

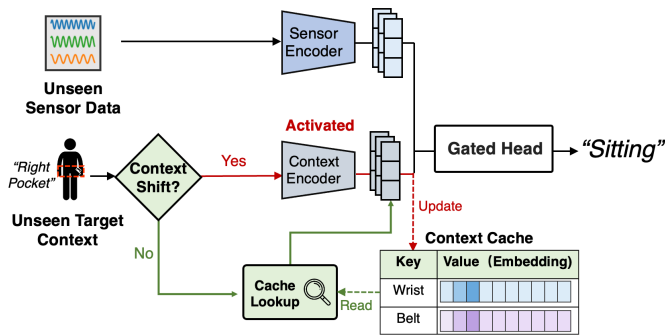


Figure 7: Dynamic context caching during inference.

environments evolve much more slowly than packet-level traffic.

Let the streaming input at time step  $t$  be  $(x_t, u_t)$ , where  $x_t$  is the current sensor sample and  $u_t$  is the associated context identifier, such as a placement label or environment tag. Chorus maintains the cached context representation from the previous step and updates it only when the context identifier changes:

$$z_t^c = \begin{cases} z_{t-1}^c, & \text{if } u_t = u_{t-1}, \\ f_{\text{context}}(c(u_t)), & \text{if } u_t \neq u_{t-1}. \end{cases}$$

That is, if the current context matches the cached one, Chorus directly reuses the previous latent context feature; otherwise, it recomputes the context representation and refreshes the cache. This changes context encoding from a per-sample operation to an event-driven update. For a stream with  $T$  samples and only  $M$  context changes, the number of context-encoding operations is reduced from  $T$  to  $M + 1$ .

For example, in an IMU activity-recognition session where a wearable remains on the *Wrist* for 500 consecutive samples, a naive design would invoke the context branch 500 times, while Chorus encodes the *Wrist* descriptor once and reuses the cached latent vector for the remaining 499 samples. Similarly, in speech enhancement, if the environment remains *Bus* for a long interval and switches to *Office* only once, the context encoder is executed only at the two segment boundaries rather than for every audio chunk.

The cache stores the output of the full context-processing stack after adaptation and normalization, so that all subsequent steps reuse the same control feature. This mechanism reduces both latency and energy consumption on resource-constrained edge devices without changing the downstream gating behavior when the context remains unchanged. The cache key  $u_t$  can be obtained either from explicit deployment metadata or from a lightweight context detector, as described next.

**Context acquisition and detection.** Chorus exploits a lightweight context signal at inference time, which can

Dataset	Modality	Task	Context (#)	# of subjects
Shoab [28]	IMU	HAR	Placement (5)	10
VoiceBank-DEMAND [33]	Speech	Enhancement	Environment (10)	30
CSI-Bench [47]	WiFi	Fall Detection	Environment (6)	17

Table 1: Summary of datasets used in the evaluation.

be obtained in two practical ways. The first is directly acquired context, utilizing deployment metadata, OS/device tags, or explicit user setup. For example, IMU on-body placements such as “Wrist” and “Belt” can be provided directly via wearable OS metadata or initialized through a lightweight few-sample calibration [28]. The second is detected context, produced by a lightweight background classifier running on commodity signals. For instance, in our speech and WiFi pipelines, ambient environments such as “Bus” or “Office” are opportunistically inferred from low-power smartphone signals, such as WiFi scans or coarse audio statistics, following the StudentLife sensing paradigm [36]. In our system evaluations, this lightweight front-end classifier achieves an automated detection accuracy of 87.25%, serving as a realistic operating point for edge deployments.

Regardless of the acquisition method, the resulting context is formatted as a short language descriptor and encoded by  $f_{\text{context}}$ . This design decouples context acquisition from the neural architecture, so that the downstream model consumes context in a uniform format.

## 6 EVALUATION

### 6.1 Methodology

**6.1.1 Datasets.** We use three public datasets covering inertial sensing, speech, and WiFi signals (Table 1). We use Shoab with on-body placement as context, VoiceBank-DEMAND with noise types as acoustic context, and the FallDetection subset of CSI-Bench with environment as context. Table 2 summarizes the source–target context splits and latent MMD values used to construct the Low/Mid/High shift settings.

**6.1.2 Experimental Settings.** To study robustness under controlled context shifts, we construct Low/Mid/High tiers using latent-MMD distances between fixed source contexts and unseen target contexts (Table 2). For each modality, we use two source contexts for training and one held-out target context for testing in each tier. We pre-train the context-aware encoder on the 80% training split of the source contexts and train the adaptive head with 1/2/5/10% labeled source data from the same contexts. Unless otherwise noted, all results follow a strict source-only protocol without target-domain data; §6.2 separately studies limited target-label adaptation. For gating, we use modality-appropriate masks over the shared feature pool rather than enforcing the same

Modality	Source contexts	Target	Shift	Latent MMD
IMU	left/right pocket	wrist	Low	0.587
		upper arm	Mid	0.873
		belt	High	1.571
Speech	kitchen, restaurant	living room	Low	0.095
		bus	Mid	0.194
		office	High	0.202
WiFi	large house, office	medium house	Low	0.067
		apartment	Mid	0.100
		villa	High	0.214

**Table 2: Settings of context shifts for different datasets.**

cues across all modalities: IMU and WiFi mainly use dynam-ics+uncertainty, while speech mainly uses alignment.

**6.1.3 Baselines.** We compare Chorus against Sensor-Only, fixed context fusion baselines (Fix-Add, Fix-Concat, Fix-Attn), supervised contrastive learning (SupCon), source-only pre-train/fine-tune baselines (TS-TST), domain-adaptation-style baselines (M3BAT, ContrasGAN), and a context-specialist baseline (CACTUS). Unless otherwise noted, all methods are trained under the same source-only protocol and source-label budgets. For methods originally designed for target-aware adaptation, we evaluate their source-only variants for fair comparison.

**6.1.4 Configurations.** Within each modality, we use a compact 1D CNN backbone for IMU HAR and a Transformer encoder for speech enhancement and WiFi fall detection, with shared hidden dimensions and depth across methods.<sup>2</sup> For Chorus, the context-aware encoder is pre-trained on the 80% source-context split and the adaptive head is fine-tuned on 1/2/5/10% labeled source data. Pre-training and fine-tuning both run for up to 100 epochs with patience 15. Batch size and learning rate are fixed per modality across all source-budget settings (IMU: 32 and  $10^{-4}$ ; WiFi: 64 and  $5 \times 10^{-5}$ ; Speech: 2 and  $5 \times 10^{-5}$ ). We report accuracy for IMU/WiFi, and PESQ for speech.

**6.1.5 Implementation.** We deploy Chorus on two commodity smartphones for IMU HAR: an iPhone 16 Pro running CoreML and a Xiaomi 14 running ONNX Runtime Mobile. On both platforms, inference runs on CPU for controlled comparison, with simple sensor-wise IMU calibration before inference.

<sup>2</sup>TS-TST [43] is the only baseline that requires its own Transformer-based architecture.

## 6.2 Overall Performance

We compare Chorus and the baselines across modalities and context-shift levels under the source-only customization setting. Figure 8 fixes the labeled source budget to 10% and varies the degree of context shift, while Figure 9 focuses on the hardest IMU target (*Belt*) under different source-label budgets and limited target-label adaptation. Results in these source-budget sweeps are averaged over three random seeds with standard-deviation error bars.

**6.2.1 Performance across different degrees of context shift.** With 10% labeled source data, Chorus remains strong as context shift increases. On IMU and WiFi, it outperforms the strongest baseline across all three shift tiers, with the clearest margin on IMU Low shift, where it improves over CACTUS by 20.2%. Generic adversarial and contrastive baselines can remain competitive under lighter shifts, but degrade more noticeably as the shift becomes stronger.

On speech enhancement, Chorus remains competitive in the Low and Mid tiers and achieves the best result under the High shift. This pattern suggests that the benefit of aligned context representations becomes most visible when unseen shifts are strong enough that source-only transfer becomes less reliable. Across modalities, the gains are most consistent on IMU and WiFi, while speech shows a smaller margin when the strongest source-only baseline is already competitive. Overall, these results suggest that aligned context representations are most useful under stronger unseen shifts, where fixed fusion and generic source-only baselines become less reliable.

**6.2.2 Performance with different amounts of data.** We next vary the labeled source-data budget on the hardest IMU target (*Belt*). As shown in Figure 9(a), Chorus remains the strongest method across all budgets, but its performance is not monotonic: it improves from 1% to 5% and then drops at 10%, where the cross-seed variance is also the largest. This suggests that under severe unseen shift, more labeled source data does not necessarily improve target-context generalization and may instead increase over-specialization to source-context-specific patterns.

**6.2.3 Few-shot test-time adaptation under the hardest shift.** We further examine the same source-trained Chorus model when a small amount of target data becomes available under the hardest IMU setting (High shift, *Belt*). At test time, we expose the model to only  $K \in \{5, 10, 20\}$  target samples per class under two settings: unlabeled target samples and labeled target samples. Chorus-OFTTA applies an OFTTA-style unlabeled adaptation protocol, while Chorus-FT performs supervised few-shot adaptation from the same source-trained initialization.

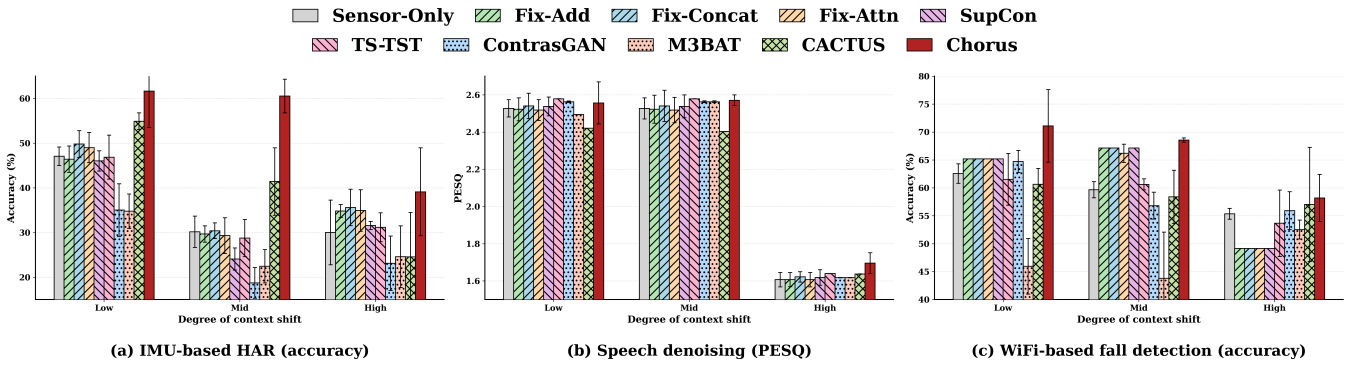


Figure 8: Performance across degrees of context shifts for IMU-based human activity recognition (HAR), speech enhancement, and WiFi-based fall detection. Error bars indicate standard deviation over three random seeds.

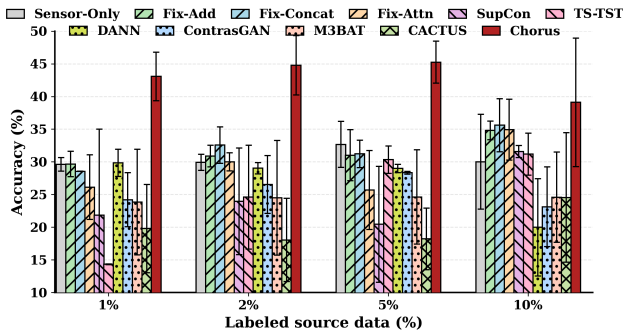
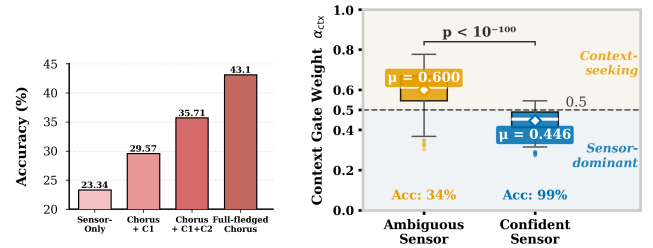
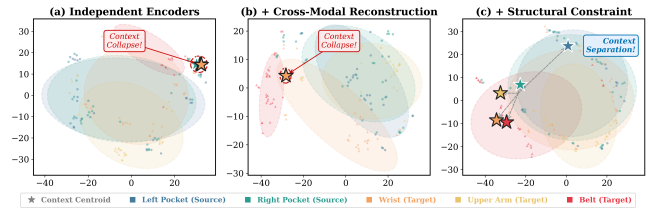


Figure 9: Performance with different amounts of labeled data. Error bars indicate standard deviation over three random seeds.



(a) Design modules. (b) Sample-level gating analysis.



(c) t-SNE [34] visualization of source/target sensor features and context centroids. Star markers denote context centroids.

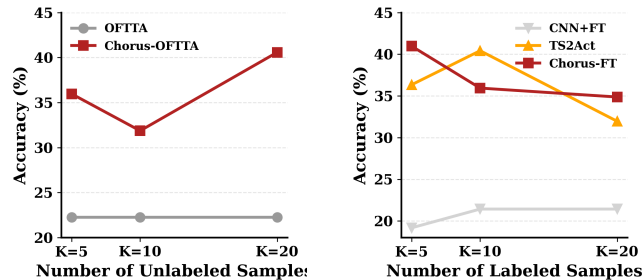
Figure 11: Understanding Chorus’s performance.

### 6.3 Understanding Chorus’s performance

We next examine which components of Chorus drive robustness under context shifts.

**6.3.1 Ablation study.** Alignment is the main source of robustness, while adaptive gating provides smaller inference-time gains. On the hardest IMU setting (1% labels, High shift), static context fusion improves the Sensor-Only backbone from 23.3% to 29.6%, and adaptive gating further raises it to 35.7%. With context-aware pre-training enabled, the full Chorus reaches 43.1%. This indicates that gating helps, but the dominant gain comes from aligned context representations.

**6.3.2 Effectiveness of context representations.** Chorus improves robustness not by simply injecting context, but by preserving a separable context geometry under unseen shifts. Ordinary cross-modal reconstruction still leads to context



(a) Unlabeled target samples. (b) Labeled target samples. Figure 10: Few-shot adaptation on the hardest IMU shift (*Belt*).

Figure 10 shows that unlabeled few-shot adaptation remains unstable under this shift. For Chorus-OFTTA, the averaged accuracy is 35.97%, 31.87%, and 40.58% at  $K = 5, 10,$  and  $20,$  respectively. The non-monotonic trend persists after averaging over three seeds, indicating strong sensitivity to the composition of the few-shot target set. This suggests that post-hoc unlabeled adaptation alone is insufficient when the source-target geometry remains substantially mismatched.

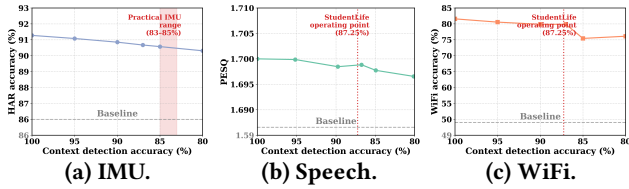


**Figure 12: Robustness to imperfect context prediction.** The horizontal dashed line in each panel marks the corresponding Sensor-Only baseline, while the red marker indicates a realistic deployment operating point.

collapse, with centroid cosine similarity increasing to 0.727 and mean pairwise L2 distance shrinking to 3.65. After adding the structural constraint, centroid cosine similarity drops to  $-0.221$  and mean pairwise L2 distance expands to 12.94, yielding much clearer placement-specific clusters in Figure 11c. Star markers denote context centroids.

**6.3.3 Effectiveness of the gating module.** The gating controller operates at the sample level rather than following a fixed environment-level policy. As shown in Figure 11b, it assigns lower context weight to high-confidence sensor samples and higher context weight to ambiguous ones. This suggests that the gate mainly serves as a reliability-aware inference-time mechanism on top of the aligned representations.

## 6.4 Robustness to imperfect context prediction

**6.4.1 Context detection operating points.** In deployment, context is typically provided by a lightweight front-end rather than oracle metadata. To evaluate this setting, we use the 10% labeled, High-shift checkpoints of Chorus and vary only the accuracy of the upstream context detector at inference time. For speech and WiFi, we use the StudentLife-style operating point of 87.25% context-detection accuracy. For IMU placement, our few-sample analysis suggests a practical deployment range of roughly 83–85% using 5–10 samples (about 1–2 s of data). These operating points are marked in Figure 12 as realistic deployment references rather than oracle settings.

**6.4.2 Impact on downstream performance.** Figure 12 shows how downstream performance changes as context-detection accuracy decreases. In each panel, the horizontal dashed line marks the corresponding Sensor-Only baseline, i.e., 30.0 for IMU, 1.59 for speech, and 49.0 for WiFi. Across all three modalities, Chorus remains above this baseline throughout the tested range, indicating that imperfect predicted context weakens the context prior but does not remove the benefit of context-aware customization.

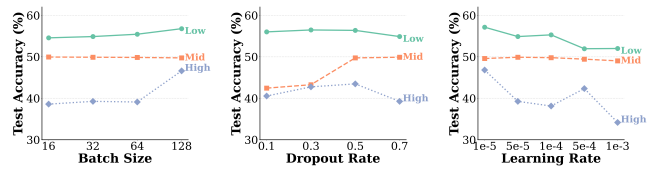


**Figure 13: Performance of Chorus with different hyperparameters.** (a) Batch size. (b) Dropout rate. (c) Learning rate.

The gap remains clear at realistic deployment points. In IMU, performance within the practical 83–85% placement-detection range stays well above the Sensor-Only baseline. In speech and WiFi, the StudentLife operating point of 87.25% also preserves a clear margin over the baseline, and performance degrades only gradually as context accuracy decreases further. This trend suggests that the effect of context noise is smooth rather than catastrophic: even when the predicted context is imperfect, the aligned sensor pathway still preserves substantial downstream task information.

## 6.5 Micro-benchmark Performance

We next analyze the sensitivity of Chorus to basic training hyperparameters in the IMU setting (Figure 13).

**6.5.1 Impact of batch sizes.** We first evaluate the accuracy with different batch sizes. The results are shown in Figure 13a. We observe that the Low and Mid tiers remain almost unchanged from batch size 16 to 128, while the High tier improves noticeably at batch size 128. This means that Chorus is generally robust to batch size, although the hardest-shift regime benefits more from a larger batch.

**6.5.2 Impact of dropout rates.** We then study the impact of dropout rate on accuracy performance. The results are shown in Figure 13b. We observe that the Low tier stays stable across different dropout settings, while the Mid and High tiers vary more visibly and perform best under moderate dropout. This means that dropout mainly affects the more challenging shift regimes, where it serves as a useful regularizer for representation learning.

**6.5.3 Impact of learning rates.** We further investigate the performance of Chorus with different learning rates. The results are shown in Figure 13c. We observe that the clearest sensitivity appears in the High tier, which performs best under the smallest learning rate and degrades under larger rates, while the Low and Mid tiers remain comparatively stable. This means that Chorus is reasonably robust across a broad range of learning rates, but the hardest-shift regime prefers a more conservative optimization setting.

Method	Params (M)	Size (MB)	Latency (ms)	Memory (MB)	Energy (mJ)
Sensor-Only	0.102	0.204	0.378	129.5	10390.9
Fix-Concat	0.177	0.349	0.358	133.7	2836.1
CACTUS	0.185	0.374	0.648	854.27	5515.7
Chorus w/o Cache	0.300	0.578	16.237	474.5	4201.6
<b>Chorus w/ Cache</b>	<b>0.300</b>	<b>0.578</b>	<b>0.547</b>	<b>470.0</b>	<b>3287.3</b>

**Table 3: Smartphone overhead on Xiaomi 14 for IMU inference.**

## 6.6 System Overhead

Beyond adaptation accuracy, practical deployment also requires low on-device overhead. We therefore evaluate IMU inference latency, memory footprint, and smartphone-side energy on commodity mobile devices. Compared with CACTUS, which uses a context-specialist design, Chorus maintains a unified generalist architecture and uses context caching to avoid repeated context encoding during streaming inference.

*6.6.1 Comparison of system overhead with baselines.* Table 3 reports Xiaomi 14 overhead for IMU inference. With caching enabled, Chorus runs at 0.547 ms latency, remaining close to lightweight baselines and below CACTUS (0.648 ms). Without caching, latency rises to 16.237 ms, indicating that the dominant overhead comes from repeated context encoding. Although Chorus keeps the context encoder loaded at runtime, it still uses substantially less memory than CACTUS on Xiaomi 14 (470.0 MB vs. 854.27 MB), because CACTUS maintains one micro classifier per context. Energy shows the same within-method trend, with caching reducing Chorus from 4201.6 mJ to 3287.3 mJ. Params and model size report the IMU inference core, while memory reports the profiler-measured runtime footprint.

*6.6.2 Impact of context caching across mobile platforms.* Table 4 shows that the benefit of caching is consistent across both smartphones. On iPhone 16 Pro, caching reduces latency from 4.342 ms to 0.184 ms; on Xiaomi 14, it reduces latency from 16.237 ms to 0.547 ms. In both cases, the cached version remains close to Sensor-Only, while the uncached version is much slower. Memory changes only slightly between cached and uncached variants on the same platform, indicating that caching mainly reduces repeated context-encoding cost rather than runtime footprint.

## 6.7 Real-world Case Study

**IMU-based HAR with Smartphones under Continuous Context Shifts.** We deploy Chorus as an iOS application via Core ML [1] on an iPhone 16 Pro. The app captures raw IMU streams at 50 Hz and performs on-device inference every 0.5 s

Platform	Approach	Latency (ms)	Memory (MB)
iPhone 16 Pro	Sensor-Only	0.141	19.5
	Chorus w/o Cache	4.342	134.5
	<b>Chorus w/ Cache</b>	<b>0.184</b>	<b>129.9</b>
Xiaomi 14	Sensor-Only	0.378	129.5
	Chorus w/o Cache	16.237	474.5
	<b>Chorus w/ Cache</b>	<b>0.547</b>	<b>470.0</b>

**Table 4: Performance in different platforms.**

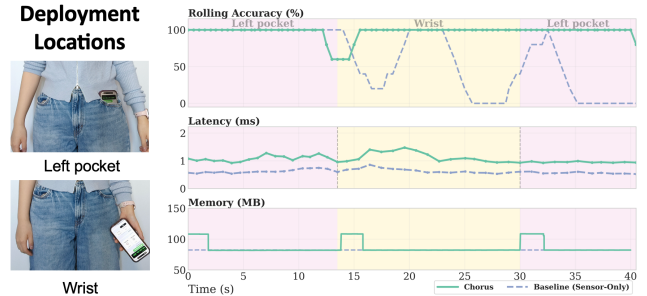


**Figure 14: Real-world IMU deployment on iPhone. Left: two practical deployment locations, *Left pocket* and *Wrist*. Right: rolling accuracy, latency, and memory during a continuous context/activity-shift demo.**

using 128-sample windows. We evaluate a continuous sequence with two practical deployment locations, *Left pocket* and *Wrist*, while the user performs *Sitting*, *Standing*, *Jogging*, and *Standing*. We compare Chorus against a Sensor-Only baseline under the same application pipeline.

Figure 14 shows that Chorus remains substantially more stable than the Sensor-Only baseline throughout the sequence. Chorus achieves 96.3% mean rolling accuracy, compared with 58.5% for the baseline, with much lower fluctuation. Although it shows a brief dip around the *Left pocket* → *Wrist* transition, it quickly recovers and maintains stable predictions. This gain comes with only a small latency overhead: Chorus reaches 1.069 ms mean latency and 1.519 ms P95, compared with 0.614 ms and 0.827 ms for Sensor-Only, while remaining comfortably real-time. Memory spikes are brief and align with context transitions, when the cached context representation is refreshed. This indicates that the additional deployment cost is concentrated at transition points rather than incurred continuously during steady-state inference.

## 7 DISCUSSION

**Generalization beyond observed source-context coverage.** Although Chorus improves robustness under unseen shifts, the aligned latent space is still learned from a finite set of source contexts, and an important next step is to better

support interpolation and extrapolation beyond the source conditions observed during training.

**Richer structure in the aligned latent space.** Our current design mainly separates known context identities and models relatively coarse context descriptions; a natural extension is to capture richer latent structure, such as continuous context variation and compositional context factors.

**Alignment under richer deployment conditions.** Another direction is to explore richer alignment cues and carefully constrained adaptation strategies, so that Chorus can maintain robust context-aware customization under more complex deployment conditions without sacrificing backbone stability.

## 8 CONCLUSION

We presented Chorus, a context-aware, data-free customization framework for IoT sensing under unseen deployment conditions. Chorus learns aligned sensor–context representations through regularized cross-modal reconstruction, and then exploits these representations with a lightweight inference-time gating module and dynamic context caching for efficient deployment. Experiments on IMU, speech enhancement, and WiFi sensing tasks show that Chorus consistently improves robustness under unseen context shifts while maintaining low latency on smartphones and edge devices.

## REFERENCES

- [1] Apple Inc. 2026. Core ML | Apple Developer Documentation. <https://developer.apple.com/documentation/coreml>. (2026). Accessed: 2026-03-11.
- [2] Trevor F. Cox and Michael A. A. Cox. 2001. *Multidimensional Scaling* (2 ed.). Chapman and Hall/CRC. <https://doi.org/10.1201/9780367801700>
- [3] Anind K. Dey, Gregory D. Abowd, and Daniel Salber. 2001. A Conceptual Framework and a Toolkit for Supporting the Rapid Prototyping of Context-Aware Applications. *Human–Computer Interaction* 16, 2–4 (2001), 97–166. [https://doi.org/10.1207/S15327051HCI16234\\_02](https://doi.org/10.1207/S15327051HCI16234_02)
- [4] Chelsea Finn, Pieter Abbeel, and Sergey Levine. 2017. Model-Agnostic Meta-Learning for Fast Adaptation of Deep Networks. In *Proceedings of the 34th International Conference on Machine Learning (Proceedings of Machine Learning Research)*, Vol. 70. PMLR, 1126–1135. <https://proceedings.mlr.press/v70/finn17a.html>
- [5] Yaroslav Ganin, Evgeniya Ustinova, Hana Ajakan, Pascal Germain, Hugo Larochelle, François Laviolette, Mario Marchand, and Victor Lempitsky. 2016. Domain-adversarial training of neural networks. *The journal of machine learning research* 17, 1 (2016), 2096–2030.
- [6] Wen Ge, Guanyi Mou, Emmanuel O. Agu, and Kyumin Lee. 2023. Deep Heterogeneous Contrastive Hyper-Graph Learning for In-the-Wild Context-Aware Human Activity Recognition. *Proceedings of the ACM on Interactive, Mobile, Wearable and Ubiquitous Technologies* 7, 4, Article 159 (2023), 159:1–159:23 pages. <https://doi.org/10.1145/3631444>
- [7] Taesik Gong, Yeonsu Kim, Jinwoo Shin, and Sung Ju Lee. 2019. MetaSense: Few-shot Adaptation to Untrained Conditions in Deep Mobile Sensing. In *Proceedings of the 17th ACM Conference on Embedded Networked Sensor Systems (SenSys '19)*. Association for Computing Machinery, 110–123. <https://doi.org/10.1145/3356250.3360020>
- [8] Arthur Gretton, Karsten M. Borgwardt, Malte J. Rasch, Bernhard Schölkopf, and Alexander Smola. 2012. A Kernel Two-Sample Test. *Journal of Machine Learning Research* 13, Mar (2012), 723–773. <http://www.jmlr.org/papers/v13/gretton12a.html>
- [9] Ishaan Gulrajani and David Lopez-Paz. 2021. In Search of Lost Domain Generalization. In *International Conference on Learning Representations (ICLR)*. <https://openreview.net/forum?id=lQdXeXDoWtI>
- [10] Wei Hao et al. 2025. Nazar: Monitoring and Adapting ML Models on Mobile Devices. In *Proceedings of the 28th ACM International Conference on Architectural Support for Programming Languages and Operating Systems (ASPLOS '25)*. Rotterdam, Netherlands. <https://www.cs.columbia.edu/~junfeng/papers/nazar-asplos25.pdf> See also preprint/PDF.
- [11] Seyed Amir Hoseini-Tabatabaei, Alexander Gluhak, and Rahim Tafazolli. 2013. A Survey on Smartphone-Based Systems for Opportunistic User Context Recognition. *Comput. Surveys* 45, 3 (2013), 27:1–27:51. <https://doi.org/10.1145/2480741.2480744>
- [12] Michael I. Jordan and Robert A. Jacobs. 1994. Hierarchical Mixtures of Experts and the EM Algorithm. *Neural Computation* 6, 2 (1994), 181–214. <https://doi.org/10.1162/neco.1994.6.2.181>
- [13] Barbara T. Korel and Simon G. M. Koo. 2010. A Survey on Context-Aware Sensing for Body Sensor Networks. *Wireless Sensor Network* 2, 8 (2010), 571–583. <https://doi.org/10.4236/wsn.2010.28069>
- [14] Manikanta Kotaru, Kiran Joshi, Dinesh Bharadia, and Sachin Katti. 2015. SpotFi: Decimeter Level Localization Using WiFi. *SIGCOMM Comput. Commun. Rev.* 45, 4 (Aug. 2015), 269–282. <https://doi.org/10.1145/2829988.2787487>
- [15] Nicholas D. Lane, Petko Georgiev, and Lorena Qendro. 2015. DeepEar: Robust Smartphone Audio Sensing in Unconstrained Acoustic Environments Using Deep Learning. In *Proceedings of the 2015 ACM International Joint Conference on Pervasive and Ubiquitous Computing (UbiComp '15)*. ACM, 283–294. <https://doi.org/10.1145/2750858.2804262>
- [16] Hansoo Lee, Joonyoung Park, and Uichin Lee. 2023. A Systematic Survey on Android API Usage for Data-driven Analytics with Smartphones. *Comput. Surveys* 55, 5 (2023), 104:1–104:38. <https://doi.org/10.1145/3530814>
- [17] Jian Liang, Ran He, and Tieniu Tan. 2025. A Comprehensive Survey on Test-Time Adaptation Under Distribution Shifts. *International Journal of Computer Vision* 133 (2025), 31–64. <https://doi.org/10.1007/s11263-024-02181-w>
- [18] Yongsen Ma, Gang Zhou, and Shuangquan Wang. 2019. WiFi Sensing with Channel State Information: A Survey. *Comput. Surveys* 52, 3 (2019), 46:1–46:36. <https://doi.org/10.1145/3310194>
- [19] Lakmal Meegahapola, Hamza Hassoune, and Daniel Gatica-Perez. 2024. M3BAT: Unsupervised Domain Adaptation for Multimodal Mobile Sensing with Multi-Branch Adversarial Training. *Proc. ACM Interact. Mob. Wearable Ubiquitous Technol.* 8, 2, Article 46 (May 2024), 30 pages. <https://doi.org/10.1145/3659591>
- [20] Fen Miao, Yayu Cheng, Yi He, Qingyun He, and Ye Li. 2015. A Wearable Context-Aware ECG Monitoring System Integrated with Built-in Kinematic Sensors of the Smartphone. *Sensors* 15, 5 (2015), 11465–11484. <https://doi.org/10.3390/s150511465>
- [21] Emiliano Miluzzo, Nicholas D. Lane, Kristóf Fodor, Ronald A. Peterson, Hong Lu, Mirco Musolesi, Shane B. Eisenman, Xiao Zheng, and Andrew T. Campbell. 2008. Sensing Meets Mobile Social Networks: The Design, Implementation and Evaluation of the CenceMe Application. In *Proceedings of the 6th ACM Conference on Embedded Networked Sensor Systems (SenSys '08)*. ACM, 337–350. <https://doi.org/10.1145/1460412.1460445>
- [22] Jiquan Ngiam, Aditya Khosla, Mingyu Kim, Juhan Nam, Honglak Lee, and Andrew Y. Ng. 2011. Multimodal Deep Learning. In *Proceedings of the 28th International Conference on Machine Learning (ICML '11)*.

689–696.

- [23] Mohammad Mehdi Rastikerdar, Jin Huang, Shiwei Fang, Hui Guan, and Deepak Ganesan. 2024. CACTUS: Dynamically Switchable Context-aware micro-Classifiers for Efficient IoT Inference. In *Proceedings of the 22nd Annual International Conference on Mobile Systems, Applications and Services, MOBISYS 2024, Minato-ku, Tokyo, Japan, June 3-7, 2024*, Tadashi Okoshi, JeongGil Ko, and Robert LiKamWa (Eds.). ACM, 505–518. <https://doi.org/10.1145/3643832.3661888>
- [24] Andrea Rosales Sanabria, Franco Zambonelli, Simon Dobson, and Juan Ye. 2021. ContrasGAN: Unsupervised domain adaptation in Human Activity Recognition via adversarial and contrastive learning. *Pervasive Mob. Comput.* 78, C (Dec. 2021), 18. <https://doi.org/10.1016/j.pmcj.2021.101477>
- [25] Mahadev Satyanarayanan. 2017. The Emergence of Edge Computing. *Computer* 50, 1 (2017), 30–39. <https://doi.org/10.1109/MC.2017.9>
- [26] Noam Shazeer, Azalia Mirhoseini, Krzysztof Maziarz, Andy Davis, Quoc V. Le, Geoffrey E. Hinton, and Jeff Dean. 2017. Outrageously Large Neural Networks: The Sparsely-Gated Mixture-of-Experts Layer. In *5th International Conference on Learning Representations (ICLR)*. <https://openreview.net/forum?id=B1ckMDqJg> Poster.
- [27] Yuge Shi, N. Siddharth, Brooks Paige, and Philip H. S. Torr. 2019. Variational Mixture-of-Experts Autoencoders for Multi-Modal Deep Generative Models. In *Advances in Neural Information Processing Systems (NeurIPS)*.
- [28] Muhammad Shoaib, Hans Scholten, and P.J.M. Havinga. 2013. Towards Physical Activity Recognition Using Smartphone Sensors. In *2013 IEEE 10th International Conference on Ubiquitous Intelligence and Computing and 2013 IEEE 10th International Conference on Autonomic and Trusted Computing*. 80–87. <https://doi.org/10.1109/UIC-ATC.2013.43>
- [29] Masahiro Suzuki, Kohei Nakayama, and Yutaka Matsuo. 2016. Joint Multimodal Learning with Deep Generative Models. *arXiv preprint arXiv:1611.01891* (2016).
- [30] Timo Sztyler, Heiner Stuckenschmidt, and Wolfgang Petrich. 2017. Position-aware Activity Recognition with Wearable Devices. *Pervasive and Mobile Computing* 38 (2017), 281–295. <https://doi.org/10.1016/j.pmcj.2016.10.012>
- [31] Jiaqi Tang et al. 2024. AdaShadow: Responsive Test-time Adaptation for Non-stationary Mobile Environments. In *Proceedings of the 22nd ACM Conference on Embedded Networked Sensor Systems (SenSys '24)*. Association for Computing Machinery, New York, NY, USA, 14. <https://doi.org/10.1145/3666025.3699339>
- [32] Yonatan Vaizman, Nadir Weibel, and Gert R. G. Lanckriet. 2017. Context Recognition In-the-Wild: Unified Model for Multi-Modal Sensors and Multi-Label Classification. *Proceedings of the ACM on Interactive, Mobile, Wearable and Ubiquitous Technologies* 1, 4, Article 168 (2017), 168:1–168:22 pages. <https://doi.org/10.1145/3161192>
- [33] Cassia Valentini-Botinhao, Xin Wang, Shinji Takaki, and Junichi Yamagishi. 2016. Investigating RNN-based speech enhancement methods for noise-robust Text-to-Speech. In *Proceedings of the 9th ISCA Workshop on Speech Synthesis Workshop (SSW-9)*. 146–152. <https://doi.org/10.21437/SSW.2016-24>
- [34] Laurens van der Maaten and Geoffrey Hinton. 2008. Visualizing Data using t-SNE. *Journal of Machine Learning Research* 9, 86 (2008), 2579–2605. <https://www.jmlr.org/papers/v9/vandermaaten08a.html>
- [35] Dequan Wang, Evan Shelhamer, Shaoteng Liu, Bruno Olshausen, and Trevor Darrell. 2021. Tent: Fully Test-time Adaptation by Entropy Minimization. In *International Conference on Learning Representations (ICLR)*. <https://doi.org/10.48550/arXiv.2006.10726> ICLR 2021 Spotlight; arXiv:2006.10726.
- [36] Rui Wang, Fanglin Chen, Zhenyu Chen, Tianxing Li, Gabriella Harari, Samuel Tignor, Xia Zhou, Dror Ben-Zeev, and Andrew T. Campbell. 2014. StudentLife: Assessing Mental Health, Academic Performance and Behavioral Trends of College Students using Smartphones. In *Proceedings of the 2014 ACM International Joint Conference on Pervasive and Ubiquitous Computing (UbiComp '14)*. ACM, 3–14.
- [37] Shuoyuan Wang, Jindong Wang, Huajun Xi, Bob Zhang, Lei Zhang, and Hongxin Wei. 2023. Optimization-Free Test-Time Adaptation for Cross-Person Activity Recognition. *Proc. ACM Interact. Mob. Wearable Ubiquitous Technol.* 7, 4 (2023), 183:1–183:27. <https://doi.org/10.1145/3631450>
- [38] Wenhui Wang, Furu Wei, Li Dong, Hangbo Bao, Nan Yang, and Ming Zhou. 2020. MiniLM: Deep Self-Attention Distillation for Task-Agnostic Compression of Pre-Trained Transformers. In *Advances in Neural Information Processing Systems*, Vol. 33.
- [39] Kang Xia, Wenzhong Li, Shiwei Gan, and Sanglu Lu. 2023. TS2ACT: Few-Shot Human Activity Sensing with Cross-Modal Co-Learning. *Proc. ACM Interact. Mob. Wearable Ubiquitous Technol.* 7, 4 (2023), 188:1–188:22. <https://doi.org/10.1145/3631445>
- [40] Bufang Yang, Lixing He, Neiweng Ling, Zhenyu Yan, Guoliang Xing, Xian Shuai, Xiaozhe Ren, and Xin Jiang. 2024. EdgeFM: Leveraging Foundation Model for Open-set Learning on the Edge. In *Proceedings of the 21st ACM Conference on Embedded Networked Sensor Systems (SenSys '23)*. Association for Computing Machinery, New York, NY, USA, 111–124. <https://doi.org/10.1145/3625687.3625793>
- [41] Shuochao Yao, Yiran Zhao, Huajie Shao, Aston Zhang, Chao Zhang, Shen Li, and Tarek F. Abdelzaher. 2018. RDeepSense: Reliable Deep Mobile Computing Models with Uncertainty Estimations. *Proceedings of the ACM on Interactive, Mobile, Wearable and Ubiquitous Technologies* 1, 4, Article 173 (2018), 173:1–173:26 pages. <https://doi.org/10.1145/3161181>
- [42] X. Yi, Z. Chen, M. Ma, X. Wu, and Y. Xu. 2021. Cross-modal Variational Auto-encoder for Content-based Micro-video Background Music Recommendation. *IEEE Transactions on Multimedia* (2021). to appear / early access.
- [43] George Zerveas, Srideepika Jayaraman, Dhaval Patel, Anuradha Bhamidipaty, and Carsten Eickhoff. 2021. A Transformer-based Framework for Multivariate Time Series Representation Learning. In *Proceedings of the 27th ACM SIGKDD Conference on Knowledge Discovery & Data Mining (KDD '21)*. Association for Computing Machinery, New York, NY, USA, 2114–2124. <https://doi.org/10.1145/3447548.3467401>
- [44] Han Zhao, Remi Tachet des Combes, Kun Zhang, and Geoffrey J. Gordon. 2019. On Learning Invariant Representation for Domain Adaptation. (2019). arXiv:cs.LG/1901.09453 <https://arxiv.org/abs/1901.09453>
- [45] Kaiyang Zhou, Ziwei Liu, Yu Qiao, Tao Xiang, and Chen Change Loy. 2023. Domain Generalization: A Survey. *IEEE Trans. Pattern Anal. Mach. Intell.* 45, 4 (April 2023), 4396–4415. <https://doi.org/10.1109/TPAMI.2022.3195549>
- [46] Rui Zhou, Yu Cheng, Songlin Li, Hongwang Zhang, and Chenxu Liu. 2025. DGSense: A Domain Generalization Framework for Wireless Sensing. (2025). <https://doi.org/10.48550/arXiv.2502.08155> arXiv:cs.LG/2502.08155 arXiv preprint.
- [47] Guozhen Zhu, Yuqian Hu, Weihang Gao, Wei-Hsiang Wang, Beibei Wang, and K. J. Ray Liu. 2025. CSI-Bench: A Large-Scale In-the-Wild Dataset for Multi-task WiFi Sensing. *arXiv preprint arXiv:2505.21866* (2025).